nature physics

Article

https://doi.org/10.1038/s41567-023-02235-9

Resonant enhancement of photo-induced superconductivity in K_3C_{60}

Received: 18 January 2023

Accepted: 29 August 2023

Published online: 05 October 2023

Check for updates

E. Rowe[1], B. Yuan[1], M. Buzzi[1], G. Jotzu[1], Y. Zhu[1], M. Fechner[1], M. Först[1], B. Liu[1,2], D. Pontiroli[3], M. Riccò[3] & A. Cavalleri[1,4]

Photo-excitation at terahertz and mid-infrared frequencies has emerged as an effective way to manipulate functionalities in quantum materials, in some cases creating non-equilibrium phases that have no equilibrium analogue. In K_3C_{60}, a metastable zero-resistance phase was observed that has optical properties, nonlinear electrical transport and pressure dependencies compatible with non-equilibrium high-temperature superconductivity. Here we demonstrate a two-orders-of-magnitude increase in photo-susceptibility near 10 THz excitation frequency. At these drive frequencies, a metastable superconducting-like phase is observed up to room temperature. The discovery of a dominant frequency scale sheds light on the microscopic mechanism underlying photo-induced superconductivity. It also indicates a path towards steady-state operation, limited at present by the availability of a suitable high-repetition-rate optical source at these frequencies.

The search for new non-equilibrium functional phases in quantum materials, such as optically induced ferroelectricity[1,2], magnetism[3–5], charge density wave order[6,7], non-trivial topology[8,9] and superconductivity[10–18], has become a central research theme in condensed-matter physics. In the case of K_3C_{60} (Fig. 1a), mid-infrared optical pulses have been extensively documented to yield an unconventional non-equilibrium phase that exhibits metastable zero resistance[14], extraordinarily high mobility and a superconducting-like gap in the optical conductivity[12,14] that reduce with applied pressure[13], and nonlinear current–voltage characteristics[19]. All these observations are indicative of non-equilibrium high-temperature superconductivity, observed at base temperatures far exceeding the highest equilibrium superconducting critical temperature of any alkali-doped fulleride (Fig. 1b).

Typical experimental results reported until now are displayed in Fig. 2c. K_3C_{60} powders were held at a base temperature $T = 100\ \mathrm{K} \gg T_c = 20\ \mathrm{K}$ and irradiated with 1-ps-long pulses with 170 meV photon energy (wavelength $\lambda \approx 7.3\ \mu\mathrm{m}$, frequency $f \approx 41\ \mathrm{THz}$) at a fluence of 18 mJ cm^{-2}. This strong excitation regime yielded a long-lived transient state with pronounced changes in both the real and imaginary parts of the optical conductivity, measured using phase-sensitive terahertz time-domain spectroscopy. The transient optical properties displayed in Fig. 2c are reminiscent of those of the equilibrium superconducting state measured in the same material at $T \ll T_c = 20\ \mathrm{K}$ (cf. Fig. 2b) and are suggestive of transient high-temperature superconductivity. These signatures consist of perfect reflectivity, a gap in the real part of the optical conductivity $\sigma_1(\omega)$ and an imaginary conductivity $\sigma_2(\omega)$ that diverges towards low frequencies as $\sigma_2(\omega) \propto 1/\omega$. The divergent $\sigma_2(\omega)$ implies (through Kramers–Kronig relations) the presence of a peak in σ_1 centred at zero frequency, with a width limited by the lifetime of the state that also determines the carrier mobility.

These data were obtained by accounting for the inhomogeneous excitation of the probed volume using a multilayer model. Here we show the results of this reconstruction under the assumption of a linear (filled blue circles) and sublinear (open symbols)[20] dependence of the photo-induced changes in the terahertz refractive index on the mid-infrared pump fluence. Two sublinear models are shown, with an assumed square-root fluence dependence in blue circles and saturating fluence dependence in brown triangles, as detailed in Supplementary Section 6. Allowing for a finite-temperature superconductor in which a varying density of uncondensed quasiparticles also contributes

[1]Max Planck Institute for the Structure and Dynamics of Matter, Hamburg, Germany. [2]Paul Scherrer Institute, Villigen, Switzerland. [3]Dipartimento di Scienze Matematiche, Fisiche e Informatiche, Università degli Studi di Parma, Parma, Italy. [4]Department of Physics, Clarendon Laboratory, University of Oxford, Oxford, UK. e-mail: andrea.cavalleri@mpsd.mpg.de

https://doi.org/10.1038/s41567-023-02235-9

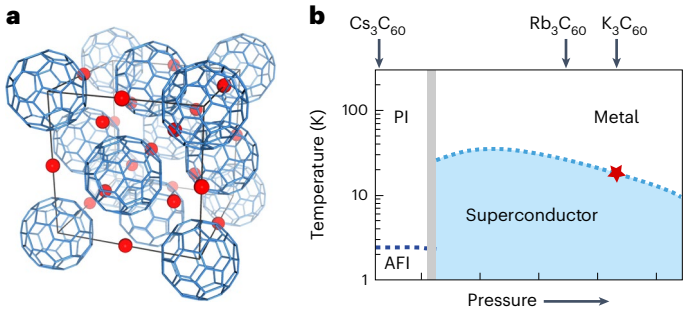

Fig. 1 | Crystal structure and phase diagram of K_3C_{60}. a, Crystal structure of the organic molecular solid K_3C_{60}. C_{60} molecules are situated at the vertices of a face-centred-cubic lattice. Potassium atoms (red) occupy the interstitial voids. **b**, Pressure–temperature phase diagram of the fcc-A_3C_{60} alkali-doped fulleride family of compounds showing the presence of superconducting, metallic, paramagnetic insulating (PI) and anti-ferromagnetic insulating (AFI) phases. Physical pressure tunes the spacing between the C_{60} molecules. The grey line indicates the boundary between the insulating and metallic/superconducting compounds. The blue shaded area indicates where superconductivity is observed at equilibrium. The star indicates the K_3C_{60} compound investigated in this work, which superconducts below the critical temperature (T_c) of 20 K.

to the terahertz response, the superconducting-like nature of the transient state is independent of the specific choice of assumption[21]. Only quantitative differences associated with the relative densities of induced superfluid and heated quasiparticles, which can be extracted by fitting with a two-fluid model, emerge. This modelling also reveals that the enhancement of conductivity observed in these experiments is connected not to an increase in the carrier density, which remains constant upon photo-excitation, but rather to a giant increase in the carrier mobility.

Three spectrally integrated figures of merit are extracted from the snapshots of reflectivity ($R(\omega,\tau)$), $\sigma_1(\omega,\tau)$ and $\sigma_2(\omega,\tau)$ and plotted as a function of pump-probe time delay τ in Fig. 2e, showing the time evolution of the system. The first two quantities are the frequency-averaged values of $R(\omega)$ and $\sigma_1(\omega)$ from 5 to 10 meV, a frequency range that lies below the photo-induced energy gap, for which a zero-temperature superconductor with infinite lifetime would give values of 1 and 0, respectively. The third figure of merit is the fractional superfluid density, which is proportional to the divergence of $\sigma_2(\omega)$. This is determined by fitting the photo-excited optical properties with a two-fluid model where one fluid represents the remaining normal carriers with a finite scattering rate and the other has zero scattering rate, giving a superconducting-like contribution. Details of this fitting procedure are given in Supplementary Section 7.

For low excitation fluences, the system becomes superconducting-like after photo-excitation and relaxes on a time scale of a few picoseconds. As already seen in the spectrally resolved measurements, for high excitation fluences, the system enters a metastable regime in which the superconducting-like optical properties persist for much longer times, up to several nanoseconds.

We note that the temperature dependence reported in ref. 12 shows transient superconducting-like optical properties up to a temperature of 150–200 K. For higher temperatures, the gapping and extracted superfluid density are severely reduced. Examples of such spectra measured at room temperature are shown in Fig. 2d. Nevertheless, the pressure scaling reported in ref. 13 suggests that traces of non-equilibrium superconductivity may survive up to higher temperatures, raising the prospect that with more effective driving, a full manifestation of the metastable superconducting-like state may be possible at 300 K.

Until now, these experiments have been limited to excitation photon energies between 80 and 165 meV (20–40 THz), such that a more comprehensive search for a dominant excitation frequency scale has remained out of reach. Many potentially important resonances at lower frequencies ($h\nu < 80$ meV) have remained unexplored, primarily due to the lack of a suitable high-intensity pump source that operates in this range. In the present work, we explore excitation at energies between 24 and 80 meV (6–20 THz). This energy range hosts many excitations, both vibrational (phonons) and electronic in nature, including a broad polaronic peak seen in σ_1 centred at about 60 meV (15 THz). The possible relevance of this excitation has been highlighted in ref. 22, although this prediction could not be tested to date.

To achieve wide tuneability, we used a terahertz source based on chirped-pulse difference frequency generation, mixing the near-infrared signal beams of two phase-locked optical parametric amplifiers[23]. This source, illustrated schematically in Fig. 3a and described in detail in Supplementary Section 4, was used to generate narrow-bandwidth pulses with photon energies spanning the range from 24 to 145 meV (6–35 THz). All measurements reported here were carried out with an excitation bandwidth of $h\Delta\nu_{pump} \approx 4$ meV (1 THz) and $\Delta\tau_{pump} \approx 600$ fs pulse duration. The same probing protocol as that reported in Fig. 2 was used here to detect changes in the complex optical properties for probe energies spanning 4–18 meV (1–4.5 THz).

Figure 3b–d shows reflectivity and complex conductivity spectra measured after photo-excitation with pulses tuned to 41 meV photon energy ($\lambda \approx 30$ μm, $f \approx 10$ THz) at base temperatures of 100 K and room temperature, respectively. The response is very similar to the case reported in Fig. 2 for 170 meV (41 THz) excitation, manifested on metastable timescales but persisting here up to room temperature despite an excitation fluence almost two orders of magnitude weaker. Figure 3e displays the time evolution of the optical properties with a transient amplifying state at early pump-probe delays, as already reported in ref. 24, which relaxes into a metastable state with superconducting-like optical properties.

Figure 4a shows the scaling with fluence of $R(\omega)$ and $\sigma_1(\omega)$ (averaged in the 5–10 meV range), as well as the fractional superfluid density in response to photo-excitation at 170 meV (41 THz) and 41 meV (10 THz). These measurements were carried out at a pump-probe time delay of 10 ps and thus refer to the metastable phase. The figure shows how all figures of merit approach their equilibrium superconducting-state values as the fluence increases, with the fluence required being roughly 50 times less for 41 meV (10 THz) compared to 170 meV (41 THz) excitation.

Similar fluence dependence measurements were carried out by varying the photon energy of the pump and maintaining a constant 4 meV (1 THz) bandwidth with 600 fs pulse duration. For all excitation photon energies between 24 meV (6 THz) and 145 meV (35 THz), the photo-induced changes in the optical properties were qualitatively similar to those shown in Figs. 2 and 3, with only the size of the response for a given fluence differing. From each fluence dependence, we extracted a figure of merit for the photo-susceptibility, defined as the rate of depletion of spectral weight in σ_1 with excitation fluence, in the limit of low fluence (Supplementary Section 8). Plots of the pump-frequency-dependent photo-susceptibility are shown in Fig. 4b for both 10 ps and 50 ps pump-probe time delay. A peak centred at 41 meV (10 THz) with about 16 meV FWHM width is observed in these measurements. Next, we will discuss three distinct energy scales that coincide with this resonance; sequentially, they relate to 'on-ball' orbital excitations, phonons and excitons.

Superconductivity in alkali-doped fullerides is believed to be mediated by a dynamical Jahn–Teller distortion, which leads to an effective negative Hund's coupling for the orbitals of a single buckyball[25] and to a low-spin $S = 1/2$ state. A theoretical model based on this assumption has been successful at providing a quantitatively correct phase diagram for fulleride superconductors from ab initio calculations[26,27]. In this model, the local ground state of the system is a sixfold degenerate low-spin state, which features intraorbital pairs that delocalize over two molecular orbitals. As detailed in Supplementary

https://doi.org/10.1038/s41567-023-02235-9

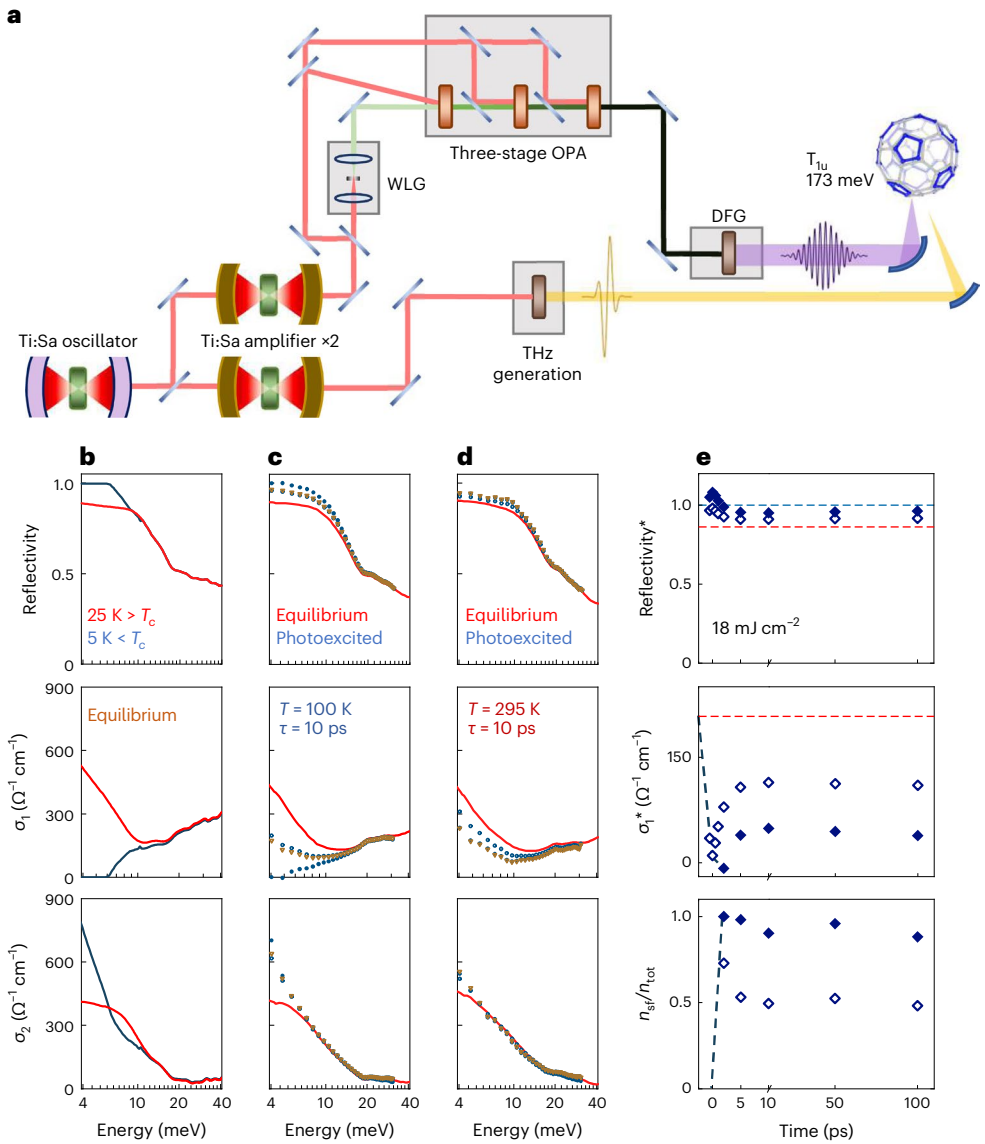

Fig. 2 | Photo-induced metastable superconductivity in K_3C_{60} generated with intense 170 meV excitation pulses. a, Schematic of the experimental setup. Pump pulses with 170 meV (41 THz) photon energy (close to resonance with the illustrated phonon mode) were generated by means of white light generation (WLG), followed by optical parametric amplification (OPA) and subsequent difference frequency generation (DFG) of the signal and idler beams. These pulses were stretched to a duration of $\Delta\tau_{pump} \approx 1$ ps by propagation in a highly dispersive CaF_2 rod. The photo-induced changes in the far-infrared optical properties of K_3C_{60} were detected with phase-sensitive transient terahertz (THz) time-domain spectroscopy. **b**, Reflectivity (sample–diamond interface) and real and imaginary parts of the optical conductivity of K_3C_{60} measured after cooling across the equilibrium superconducting transition. **c**, Same quantities measured at equilibrium (red lines) and 10 ps after excitation (symbols). The data in filled blue circles, open blue circles and open brown triangles were obtained accounting for the inhomogeneous excitation of the probed volume under the assumption of a linear, square-root and saturating (respectively) fluence dependence of the photo-induced changes in the complex refractive index of the material (Supplementary Section 6). These data were acquired at a base temperature $T = 100$ K with an excitation fluence of approx. 18 mJ cm^{-2}. **d**, Same quantities as in **c** but measured at a base temperature $T = 295$ K with an excitation fluence of approx. 15 mJ cm^{-2}. **e**, Time dependence of the average value (indicated by *) of reflectivity and real part of the optical conductivity $\sigma_1(\omega)$ in the 5–10 meV spectral range, and light-induced 'superfluid density' (n_{sf}) extracted from a two-fluid model fit and expressed as a fraction of the total charge carrier density (n_{tot}). Filled and open symbols indicate the results of the linear and square-root reconstruction models, respectively. The red dotted lines indicate the value of the corresponding quantity in equilibrium. These data were acquired at a base temperature $T = 100$ K with a fluence of approximately 18 mJ cm^{-2} and a pump-pulse duration of $\Delta\tau_{pump} \approx 1$ ps. Transient optical spectra corresponding to these measurements are reported in Supplementary Fig. 6.3.

Section 10, a first set of local excited states also features such pairs, albeit with a different angular momentum (that is, a different interorbital phase for the delocalized pair). Ab initio calculations predict an energy splitting of 37 meV between these two sets of states[26,27]. The observed resonance may therefore be related to the creation of interorbital pairs with local angular momentum, which may also contribute to superconductivity, as suggested in the Suhl–Kondo mechanism[28–30]. However, it is not yet clear exactly how this excitation is transformed in the presence of tunnelling between neighbouring C_{60} molecules and why the creation of such pairs may support metastable superconductivity at such high temperatures. Furthermore, as the local parity of this excited state would be different from that of the ground state, condensation in this configuration may give rise to a superconductor with different symmetry. This possibility, whilst tantalizing, remains speculative and should be tested with more comprehensive ultrafast probing methods.

https://doi.org/10.1038/s41567-023-02235-9

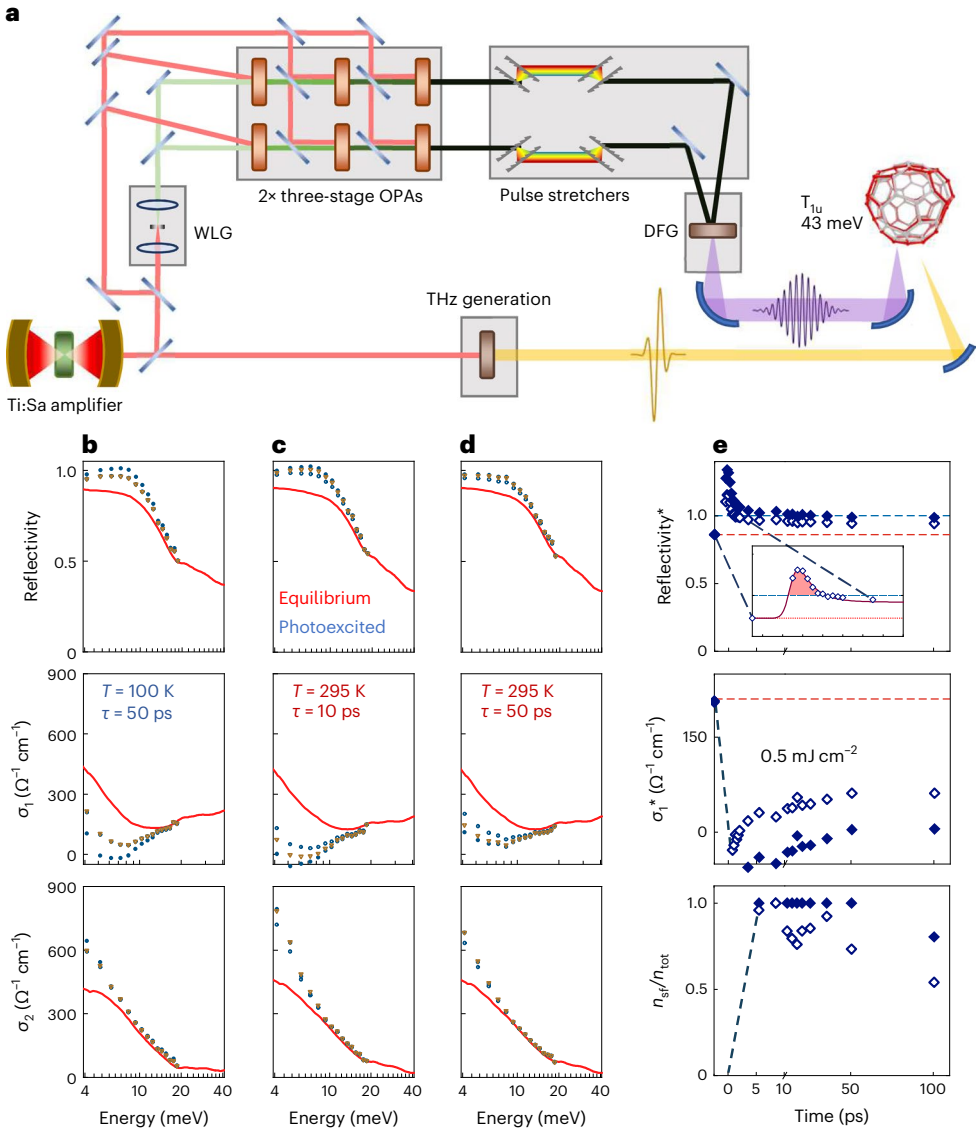

Fig. 3 | Photo-induced metastable superconductivity in K_3C_{60} generated with 41 meV excitation pulses. a, Schematic of the experimental setup. Pump pulses with 41 meV (10 THz) photon energy (close to resonance with the illustrated phonon mode) are generated using twin optical parametric amplifiers (OPAs) seeded by the same white light (WLG) through subsequent chirped-pulse difference frequency generation (DFG) of the two stretched signal beams. The photo-induced changes in the far-infrared optical properties of K_3C_{60} are detected with phase-sensitive transient terahertz time-domain spectroscopy. **b**, Reflectivity (sample–diamond interface) and real and imaginary parts of the optical conductivity of K_3C_{60} measured in equilibrium (red lines) and 50 ps after excitation (symbols). The data in filled blue circles, open blue circles and open brown triangles were obtained accounting for the inhomogeneous excitation of the probed volume under the assumption of a linear, square-root and saturating (respectively) fluence dependence of the photo-induced changes in the complex refractive index of the material (Supplementary Section 6). These data were acquired at base temperature $T = 100$ K with pump pulses tuned to 41 meV (10 THz) centre frequency and excitation fluence of approx. 0.4 mJ cm^{-2}. **c**, Same quantities as in **b** but measured 10 ps after photo-excitation at base temperature $T = 295$ K. **d**, Same quantities as in **c** but measured 50 ps after photo-excitation. **e**, Time dependence of the average value (indicated by *) of reflectivity and real part of the optical conductivity $\sigma_1(\omega)$ in the 5–10 meV spectral range, and light-induced 'superfluid density' (n_{sf}) extracted from a two-fluid model fit and expressed as a fraction of the total charge carrier density (n_{tot}). Filled and open symbols indicate the results of the linear and square-root reconstruction models, respectively. The inset in the top panel highlights the early time delays for which light amplification ($R > 1$) is observed (red shading). The red dotted lines indicate the value of the corresponding quantity in equilibrium. These data were acquired at a base temperature $T = 100$ K with pump pulses tuned to 45 meV (11 THz) photon energy and excitation fluence of approximately 0.5 mJ cm^{-2}. Frequency-resolved spectra corresponding to these measurements can be seen in Supplementary Fig. 6.4.

Turning to phonon excitations, we also note that the 41 meV resonance frequency identified here coincides with an infrared-active T_{1u} phonon, which predominantly consists of intramolecular motion of the C atoms. Whereas the atomic motions of the 170 meV molecular mode discussed previously in ref. 12 are directed along the tangential directions of the C_{60}^{3-} molecule, those of the 41 meV mode are predominantly along the radial directions (Supplementary Section 9). By performing frozen-phonon calculations using density functional theory (DFT), we evaluated the different effect of these distortions on the three t_{1u} molecular levels at the Fermi energy, which we map out from DFT wave functions as maximally localized Wannier functions (Supplementary Section 9). In the undistorted C_{60}^{3-} structure, these molecular levels are degenerate. Applying a distortion along a T_{1u} coordinate lifts this degeneracy, leaving a doubly degenerate t_{1u} orbital lowered in energy. This electronic configuration is prone to developing a Jahn–Teller distortion that may lead to an enhanced negative Hund's coupling, possibly facilitating the onset of

https://doi.org/10.1038/s41567-023-02235-9

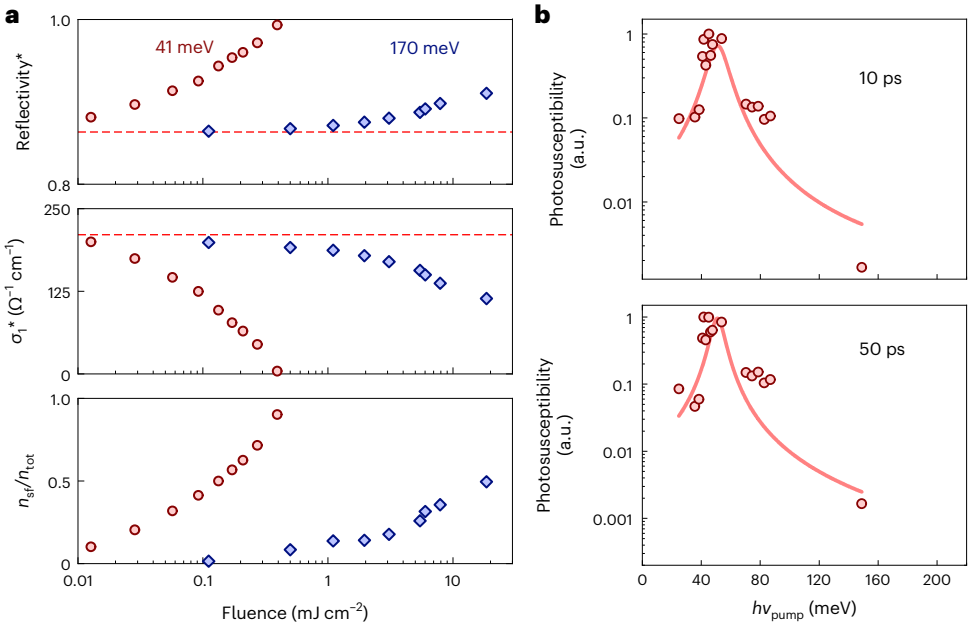

Fig. 4 | Scaling of the out-of-equilibrium features of photo-induced metastable superconductivity in K_3C_{60}. a, Fluence dependence of the average value (indicated by *) of the reflectivity and real part of the optical conductivity $\sigma_1(\omega)$ in the 5–10 meV spectral range and light-induced 'superfluid density' (n_{sf}) extracted from a two-fluid model fit and expressed as a fraction of the total charge carrier density (n_{tot}). Red and blue symbols indicate measurements with excitation pulses tuned to 41 meV (10 THz) and 170 meV (41 THz) central frequency. The red dotted lines indicate the value of the corresponding quantity at equilibrium. These data were acquired at a base temperature $T = 100$ K, at a time-delay $\Delta t = 10$ ps and with a pump-pulse duration of $\Delta\tau_{pump} \approx 600$ fs. **b**, Frequency dependence of the photo-susceptibility of K_3C_{60} defined as the gradient of the lost spectral weight in σ_1 in the low-fluence limit (Supplementary Section 8) measured 10 and 50 ps after photo-excitation. These measurements were carried out at a base temperature $T = 100$ K. These data were obtained by accounting for the inhomogeneous excitation of the probed volume under the assumption of a square-root fluence dependence of the photo-induced changes in the complex refractive index of the material. The solid curves are guides to the eye.

superconductivity at higher temperatures. The strength of the induced splitting is quadratic in the phonon coordinate and is enhanced when driving the 41 meV mode compared to the 170 meV one, suggesting that the observed resonance may arise from a more efficient manipulation of the electronic degrees of freedom when driving the 41 meV T_{1u} mode.

Finally, we address the electronic excitations discussed in ref. 22, where an enhanced effect on tuning the drive to lower frequencies was already predicted. This work proposed the existence of a dressed exciton in the excitation spectrum of K_3C_{60} at the same energy scale as the resonance reported here. Excitation of the system at this frequency would generate excitons that would act as a reservoir able to incoherently cool the quasiparticles, resulting in the reemergence of superconductivity at base temperatures in excess of the equilibrium T_c.

We expect the importance of this discovery to be capitalized on in future work. The extreme efficiency improvement due to resonant enhancement, nearing two orders of magnitude, is expected to also dramatically reduce unwanted dissipation. This, taken in conjunction with the observed nanosecond-long lifetime, suggests that excitation of the sample with a train of pulses of only 400 μJ cm^{-2} delivered at a 100 MHz repetition rate—as determined by the inverse lifetime of this state—may yield continuous wave operation. Because this effect is documented here to persist up to room temperature, continuous wave operation would likely have important practical implications. To make this regime experimentally accessible, single-order-of-magnitude improvements in the efficiency of the process or the light–matter coupling strength, combined with suitable developments in high-repetition-rate terahertz sources, would be required.

Online content

Any methods, additional references, Nature Portfolio reporting summaries, source data, extended data, supplementary information, acknowledgements, peer review information; details of author contributions and competing interests; and statements of data and code availability are available at https://doi.org/10.1038/s41567-023-02235-9.

References

1. Nova, T. F., Disa, A. S., Fechner, M. & Cavalleri, A. Metastable ferroelectricity in optically strained $SrTiO_3$. *Science* **364**, 1075–1079 (2019).
2. Li, X. et al. Terahertz field–induced ferroelectricity in quantum paraelectric $SrTiO_3$. *Science* **364**, 1079–1082 (2019).
3. Disa, A. S. et al. Polarizing an antiferromagnet by optical engineering of the crystal field. *Nat. Phys.* **16**, 937–941 (2020).
4. Wang, X. et al. Light-induced ferromagnetism in moiré superlattices. *Nature* **604**, 468–473 (2022).
5. Radu, I. et al. Transient ferromagnetic-like state mediating ultrafast reversal of antiferromagnetically coupled spins. *Nature* **472**, 205–208 (2011).
6. Kogar, A. et al. Light-induced charge density wave in $LaTe_3$. *Nat. Phys.* **16**, 159–163 (2020).
7. Wandel, S. et al. Enhanced charge density wave coherence in a light-quenched, high-temperature superconductor. *Science* **376**, 860–864 (2022).
8. Wang, Y. H., Steinberg, H., Jarillo-Herrero, P. & Gedik, N. Observation of Floquet-Bloch states on the surface of a topological insulator. *Science* **342**, 453 (2013).
9. McIver, J. W. et al. Light-induced anomalous Hall effect in graphene. *Nat. Phys.* **16**, 38–41 (2020).
10. Fausti, D. et al. Light-induced superconductivity in a stripe-ordered cuprate. *Science* **331**, 189–191 (2011).
11. Hu, W. et al. Optically enhanced coherent transport in $YBa_2Cu_3O_{6.5}$ by ultrafast redistribution of interlayer coupling. *Nat. Mater.* **13**, 705–711 (2014).

12. Mitrano, M. et al. Possible light-induced superconductivity in K_3C_{60} at high temperature. *Nature* **530**, 461–464 (2016).
13. Cantaluppi, A. et al. Pressure tuning of light-induced superconductivity in K_3C_{60}. *Nat. Phys.* **14**, 837–841 (2018).
14. Budden, M. et al. Evidence for metastable photo-induced superconductivity in K_3C_{60}. *Nat. Phys.* **17**, 611–618 (2021).
15. Buzzi, M. et al. Photo-molecular high temperature superconductivity. *Phys. Rev.* **10**, 031028 (2020).
16. Buzzi, M. et al. Phase diagram for light-induced superconductivity in κ-$(ET)_2$-X. *Phys. Rev. Lett.* **127**, 197002 (2021).
17. Cremin, K. A. et al. Photoenhanced metastable c-axis electrodynamics in stripe-ordered cuprate $La_{1.885}Ba_{0.115}CuO_4$. *Proc. Natl Acad. Sci.* **116**, 19875 (2019).
18. Isoyama, K. et al. Light-induced enhancement of superconductivity in iron-based superconductor $FeSe_{0.5}Te_{0.5}$. *Commun. Phys.* **4**, 160 (2021).
19. Wang, E. et al. Nonlinear transport in a photo-induced superconductor. Preprint at https://arxiv.org/abs/2301.06425 (2023).
20. Dodge, J. S., Lopez, L. & Sahota, D. G. Optical saturation produces spurious evidence for photoinduced superconductivity in K_3C_{60}. *Phys. Rev. Lett.* **130**, 146002 (2023).
21. Buzzi, M., Nicoletti, D., Rowe, E., Wang, E. & Cavalleri, A. Comment on arXiv:2210.01114: Optical saturation produces spurious evidence for photoinduced superconductivity in K_3C_{60}. Preprint at https://arxiv.org/abs/2303.10169 (2023).
22. Nava, A., Giannetti, C., Georges, A., Tosatti, E. & Fabrizio, M. Cooling quasiparticles in A_3C_{60} fullerides by excitonic mid-infrared absorption. *Nat. Phys.* **14**, 154–159 (2018).
23. Liu, B. et al. Generation of narrowband, high-intensity, carrier-envelope phase-stable pulses tunable between 4 and 18 THz. *Opt. Lett.* **42**, 129–131 (2017).
24. Buzzi, M. et al. Higgs-mediated optical amplification in a nonequilibrium superconductor. *Phys. Rev.* **11**, 011055 (2021).
25. Capone, M., Fabrizio, M., Castellani, C. & Tosatti, E. Strongly sorrelated superconductivity. *Science* **296**, 2364–2366 (2002).
26. Nomura, Y., Sakai, S., Capone, M. & Arita, R. Unified understanding of superconductivity and Mott transition in alkali-doped fullerides from first principles. *Sci. Adv.* **1**, e1500568 (2015).
27. Nomura, Y., Sakai, S., Capone, M. & Arita, R. Exotics-wave superconductivity in alkali-doped fullerides. *J. Phys. Condens. Matter* **28**, 153001 (2016).
28. Rice, M. J., Choi, H. Y. & Wang, Y. R. Three-band superconductivity in K_3C_{60} and Rb_3C_{60}. *Phys. Rev. B* **44**, 10414–10416 (1991).
29. Kondo, J. Superconductivity in transition metals. *Prog. Theor. Phys.* **29**, 1–9 (1963).
30. Suhl, H., Matthias, B. T. & Walker, L. R. Bardeen-Cooper-Schrieffer theory of superconductivity in the case of overlapping bands. *Phys. Rev. Lett.* **3**, 552–554 (1959).

Methods
All methods can be found in the Supplementary Information.

Data availability
Source data are provided with this paper. All other data that support the plots in this paper and other findings of this study are available from the corresponding authors upon reasonable request.

Acknowledgements
The research leading to these results received funding from the European Research Council under the European Union's Seventh Framework Programme (FP7/2007-2013)/ERC Grant Agreement No. 319286 (QMAC, A.C.). We acknowledge support from the Deutsche Forschungsgemeinschaft (DFG) through the Cluster of Excellence 'The Hamburg Centre for Ultrafast Imaging' (EXC 1074 – project ID 194651731, A.C.). We thank M. Volkmann and P. Licht for their technical assistance. We are also grateful to B. Fiedler and B. Höhling for their support in the fabrication of the electronic devices used on the measurement setup and to J. Harms for assistance with graphics.

Author contributions
E.R., B.L., M. Först, M.B. and A.C. conceived the experiment. A.C. supervised the project. The setup shown in Fig. 2 was built and related measurements were performed by M.B. and G.J. The setup shown in Fig. 3 was built by B.L. with support from M. Först, and related measurements were performed by E.R., B.Y. and Y.Z. Data analysis was performed by E.R. and M.B. K_3C_{60} samples were provided by D.P. and M.R. DFT frozen-phonon calculations were performed by M. Fechner. The single-molecule Hamiltonian treatment was developed by G.J. The manuscript was written by E.R., M.B., G.J., M. Fechner and A.C. with contributions from all other authors.

Funding
Open access funding provided by Max Planck Society.

Competing interests
The authors declare no competing interests.

Additional information
Supplementary information The online version contains supplementary material available at https://doi.org/10.1038/s41567-023-02235-9.

Correspondence and requests for materials should be addressed to A. Cavalleri.

Peer review information *Nature Physics* thanks the anonymous reviewers for their contribution to the peer review of this work.